Available online at www.sciencedirect.com
ScienceDirect
International Journal of Thermal Sciences 46 (2007) 980–988
International Journal of Thermal Sciences
www.elsevier.com/locate/ijts

Multifrequential AC modeling of the SThM probe behavior

Philippe Grossel *, Olivier Raphaël, Françoise Depasse, Thierry Duvaut, Nathalie Trannoy

Unité de Thermique et d'Analyse Physique, EA 3802, Laboratoire d'Energétique et d'Optique, Université de Reims, BP 1039, 51687 Reims cedex 2, France

Received 26 July 2006; received in revised form 28 November 2006; accepted 14 December 2006

Available online 5 February 2007

Abstract

The scanning thermal microscope is of current use for the determination of the thermal conductivity of material surfaces, with a submicrometer resolution. The determination of the parameters that have great importance in the probe response is clarified and an analytical approach in the multifrequency domain is compared with a finite element method and experimental results without contact.

Keywords: Scanning thermal microscopy; 3ω method; Thermal modeling

1. Introduction

Nowadays the Scanning Thermal Microscope (SThM) is currently used for the determination of temperature or thermal conductivity in surface physics. In particular, the AC mode is preferred *vs* the DC mode as it has been shown that the spectrum of thermal conductivities that it can measure is greater that the DC one [1,2].

On a general ground, the 3ω method is applied with success for thermo-physical parameters determination of anemometer probes, ambient gas [3,4], simple or multilayered surfaces [5–7]. In particular, a multifrequential analysis up to the third harmonic has been introduced in case of a DC plus AC current source [7]. In these works, the heating wire is considered as being homogeneous, and its junction with supplying leads is supposed as a perfect heat sink. This limits the minimization scheme to a small number of parameters (length, radius, thermal conductivity of the probe, for instance . . .).

For SThM application one must be aware that the complicated probe geometry—short bent probe, Wollaston wire, localized or non-localized contact with the sample—needs to be precisely controlled.

It must be underlined that such studies begin with the thermal probe characterization, in air, at long distance from any sample. The goal is to precisely determine the geometrical dimensions and the thermal parameters—specifically the radius and length—of the active element. The second step is the determination of the contact between the sample and the probe. This is a difficult task that is currently being analyzed at the present time [8], but this supposes a great confidence about the first step.

Thus in the present study, we only consider the first step. Our aim is to give a complete self-consistent modeling of the multifrequential behavior of the thermo-resistive probe without probe-sample contact. It takes the junction with the Wollaston wire and supplying leads into account and then precisely defines the heat sink aspect of the junction. Two different theoretical approaches are given and compared: on the one hand, a finite element analysis (FEM) will give directly the thermal response at each time; on the other hand, we propose a complete and rapid multifrequential analytical modeling that can be considered as a powerful tool for the implementation of inverse algorithms. In this paper, the customary hypothesis of an homogeneous probe (conductivity, diffusivity and exchange coefficients) is used; such an hypothesis will appear questionable.

The paper is organized as follows. The thermal probe to be modeled is presented and its description by the FEM and analytical approaches is studied. Experimental results concerning the probe in air or in a primary vacuum are compared with modelings: a necessary refinement of the local aspect (in position and time) of thermo-electrical parameters appears to be required.

* Corresponding author.
E-mail address: philippe.grossel@univ-reims.fr (P. Grossel).

1290-0729/$ – see front matter
doi:10.1016/j.ijthermalsci.2006.12.004

Nomenclature

I	electric current	A	
h	exchange coefficient	$W\,m^{-2}\,K^{-1}$	
k	1D wave vector of the thermal wave	m^{-1}	
L	lengths of the thermal fins	m	
T	difference between the temperature and the ambient one	°C	
r	radius of the fins	m	
R	electric resistance	Ω	
$\mathcal{R}$	reflection coefficient of the thermal wave at the junctions		
V	voltage between the probe extremities	V	

Greek symbols

α	thermal diffusivity	$m^2\,s^{-1}$
ε	temperature coefficient of resistivity	K^{-1}
ω	angular frequency of the current source	$rad\,s^{-1}$
κ	thermal conductivity	$W\,m^{-1}\,K^{-1}$
Φ	heat flux density	$W\,m^{-2}$
ρ	electric resistivity	Ω m

Subscripts

a	quantities at the ambient air temperature
b	AC current subscript
dc	DC current
ext	quantities relative to the constriction between the Wollaston wire and the electrical supply
p	quantities associated with the Pt–Rh probe
W	quantities associated with the Wollaston part

2. Modelings

2.1. The thermal probe

The thermal probe corresponding usually to SThM probes consists of Wollaston wire (75 μm diameter) that is bent and etched to uncover the Pt–Rh core, with 2.5 μm radius and about $2L = 200$ μm length. This uncovered core constitutes the thermal–electrical active part of SThM probe.

This probe is supplied with a given AC current, such that it is placed in conditions of the 3ω method. The device can be placed in a primary vacuum (10^{-2} Torr) or in air. The goal is here first to determine the geometrical and thermal parameters of the Pt–Rh part alone, and, in a second step to define the role and the imbalance of thermal exchange between the probe and the surrounding air.

The Wheatstone bridge permits in particular a filtering of small anharmonic components coming from resistance legs other than the probe one [Fig. 1]. In cases where the signal is in order of some μV, the voltage can be measured between the points A and B, when the bridge is balanced at the source frequency.

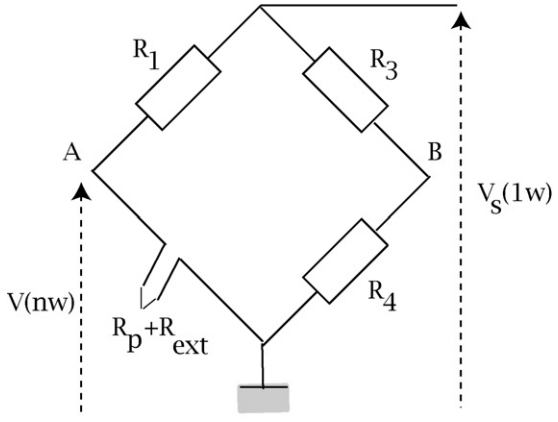

Fig. 1. The Pt–Rh probe, resistor R_p, is placed as a leg of a Wheatstone bridge. The resistance of the Wollaston wire and of the corresponding leads is R_{ext}.

In view of the inverse problem leading to the characterization of each probe (which differs one from another), a realistic analytical direct modeling is necessary. It has been known from some years that the probe can be approached in a good approximation as a thermal fin [9] leading to efficient analytical expressions. The simplest approximation consists of solving the heat equation for the thermo-resistive fin with regard to the second harmonic $T(2\omega)$ temperature field in the probe, giving the third harmonic voltage. *A priori* such an approach can be considered for low heating, but for currents that can heat the probe to more than 100 °C a self-consistent analytical solution giving a global and precise analysis of the multifrequential response is undoubtedly more satisfying.

Moreover, the Wollaston wire is usually presented in the frequency domain as a thermal perfect sink (leading to the ambient temperature for the junction Wollaston wire–probe) that simplifies analytical modelings [2–5,7,10], however some preliminary experimental infra-red analysis have shown that this is not the case, in general, due to the important length (several mm) of the Wollaston wire, before the soldering joints with the electrical supply [11]. In practice the glue and the small mirror of the probe cantilever do not constitute a sufficient thermal sink.

2.2. Finite elements method

The actual bent shape of the probe is conserved in the FEM approach to improve the confidence of the analytical fin model for comparisons with experimental data. Thus the curvature radius of Pt–Rh wire is fixed at 20 μm and its diameter and length are respectively 5 μm and 200 μm. For study of the thermal gradient in the platinum-Wollaston junction, seven millimeters of Wollaston wire are modeled. Because of planar symmetry of the SThM probe, only a hemi-probe is studied with boundary conditions of heat flux null on the symmetry plane. The structure is composed of 18 000 meshes and two nodes are separated by 1 μm in the Pt–Rh wire.

The thermal sink generated by electrical connections at the end of the Wollaston wire is modeled by an exchange coef-

ficient, h_{ext}, expressing the thermal constriction between the Wollaston wire and supplying leads at the soldering point [12]; it is estimated to be 10^7 W m^{-2} K^{-1}. The thermal power generated by Joule effect is introduced in the Pt–Rh wire taking the temperature dependence of Pt–Rh resistivity into account. The current, fixed at 50 mA, is a pure sinusoidal temporal function.

The thermal problem solved by finite elements method uses the following boundaries conditions: on lateral surface of the wires, the convective heat transfer coefficients are estimated with the classical correlation which includes a probe slope of 60 degrees *vs* the horizontal [13]. To model the radiative losses, a linearized transfer coefficient is applied to Pt–Rh wire surfaces by addition of an equivalent convective coefficient. For comparison with the analytical approach exchange coefficients of 1200 and 60 W m^{-2} K^{-1} are applied along the Pt–Rh and the Wollaston wires respectively [13]. The ambient temperature is fixed at 20 °C.

2.3. Analytical approach

2.3.1. Generalities

The challenge described in this part is the obtention of a rapid and sufficiently precise analytical method for the direct problem, which could be used systematically for the inverse one.

The multifrequential modeling works in the frame of the thermal cylindrical fin [14] and turns attention on the Pt–Rh Wollaston wire junction description. As for the FEM approach, the analytical model is limited with a hemi-probe finished by a cross-section of null thermal flux (for this non-contact study).

In the analytical modeling, it appeared that an effective constriction resistance capable of describing the thermal behavior at this junction between the two fins (of very different diameters) has great incidence with regard to comparison with the FEM response or experimental results. The junction is considered as a cone with great opening angle, described in the frame of a thermal multilayer [15] constituted from hundreds of thin cylinders with growing radius, with temperature and heat flux continuous at each interface. The geometry of the problem is finally shown on Fig. 2.

2.3.2. The multifrequential approach

Noting $T(x,t)$ the temperature difference between an element of the Pt–Rh probe and the ambient temperature, at position x and time t, the thermal problem is described by the following local Fourier equation:

$$\frac{\partial^2 T}{\partial x^2} - \frac{1}{\alpha_p}\frac{\partial T}{\partial t} - \frac{2h_p}{r_p\kappa_p}T(x,t) + \frac{\rho_a}{\pi^2 r_p^4 \kappa_p}\varepsilon T(x,t) I^2(t) = -\frac{\rho_a}{\pi^2 r_p^4 \kappa_p} I^2(t) \tag{1}$$

where κ_p and α_p are the Pt–Rh thermal conductivity and diffusivity, ρ_a the electric resistivity at the ambient temperature, and ε the temperature coefficient of the electric resistivity.

In order to solve Eq. (1) we expand the probe temperature into its time Fourier series as:

$$T(x,t) = T(x,0) + \sum_{n=1}^{\infty}\left[T(x,n\omega)\exp(-in\omega t) + T(x,-n\omega)\exp(in\omega t)\right] \tag{2}$$

As each harmonic mode satisfies Eq. (1), this equation leads by itself to a linear differential system, the dimension of which is given by the maximum value of n taken into account in expansion Eq. (2). The searched solution is a vector $T(x)$, with components $T(x,n\omega)$. The detailed analytical resolution of that constant–coefficients linear system with constant right-hand side is related in Ref. [14]. Let us only emphasize that the temperature coefficient of resistivity prevents the system from being diagonal, causing a coupling between the AC and DC modes: the lowest ω, the biggest the coupling. Fortunately, $T(x,n\omega)$ modulus rapidly decreases when n increases, allowing a cut-off expansion (Eqs. (1) and (2)); in our calculus, $n_{max} = 7$ was enough for a minimum frequency of 2 Hz.

The Wollaston part could be analyzed in the same way, but its larger diameter, *vs* the Pt–Rh probe one, leads to a negligible contribution to the Joule effect: actually, the electrical resistance of several Wollaston mm is of the order of some percents of one ohm, compared to approximatively 2 Ω of the Pt–Rh part. So the cone and the Wollaston wire will be considered as having a passive thermal behavior: for the Pt–Rh wire, it will be considered as a limit condition. The probe–cone junction is explained below: it is a simple temperature-heat flux link at the

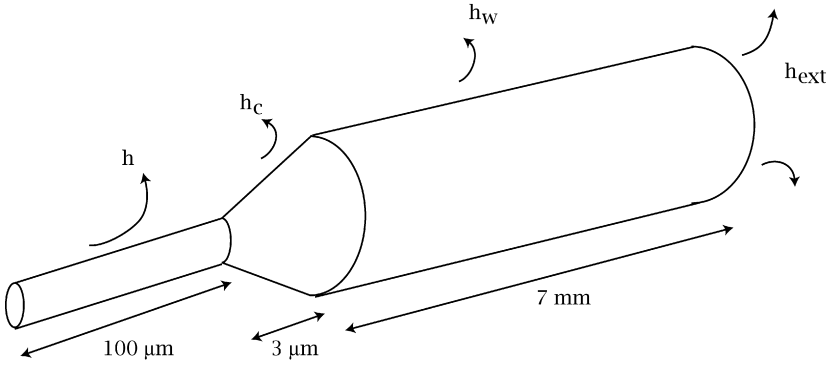

Fig. 2. The Pt–Rh probe, the junction and the Wollaston wire are modeled as successive fins. The Joule effect is considered in the Pt–Rh probe only. The exchange coefficients vary along the probe, and the thermal exchange of the Wollaston wire with the leads is expressed with an (important) exchange coefficient.

interface, taking the cone, the Wollaston wire and the external wires (heat sinks) into account.

The radiative exchange is linearized and incorporated with the convective exchange coefficient; for experiment in vacuum, its value is estimated from Stefan's law, taking the average temperature for each current into account.

Thus one can calculate the temperature field along the probe and obtain measurable parameters, as the total (variable with time) electrical resistance $R(t)$:

$$R(t) = R_a + 2\frac{\rho_a}{\pi r^2} L_p \varepsilon \langle T(t) \rangle \tag{3}$$

where $\langle T(t) \rangle$ is the x-average probe temperature at time t appearing between the SThM probe extremities. Of course, Eq. (3) introduces the Fourier component of the resistance $R(t)$, and the qth ($q = 0, \ldots, \pm n$) mode of the output voltage is obtained along $V(t) = R(t)I(t)$:

$$V(q\omega) = R(q\omega) I_{\mathrm{dc}} + \left[R\big((q-1)\omega\big) + R\big((q+1)\omega\big)\right]\frac{I_b}{2} \tag{4}$$

where the current is supposed to be $I(t) = I_{\mathrm{dc}} + I_b \cos(\omega t)$. The experimental result, at angular frequency $n\omega$, is described by:

$$V(n\omega, t) = V(n\omega)\exp(-in\omega t) + V(-n\omega)\exp(+in\omega t) \tag{5}$$

It must be underlined that, even in case of a purely AC current, Eq. (4) shows that the 3ω response incorporates the temperature fields at 2 and 4ω. This clearly appears on numerical results from the FEM or analytical approaches. For instance, typically, for a purely cosine electric current ($I_{\mathrm{dc}} = 0$), at 80 Hz frequency, $I_b = 50$ mA, the average temperature field at 4ω is in order 5% of the 2ω one; thus the coupled multifrequential response must be considered in the analysis of very stable, repetitive and sensitive signals obtained for experiments with the probe in air or vacuum without contact with sample. The different voltages, at angular frequencies ω, 3ω, 5ω, etc., can be compared with the analysis by Fourier transform of the voltage furnished by the FEM treatment, or the experimental output voltage at the lock-in amplifier, in case of AC or DC currents.

2.3.3. Junction between the Pt–Rh and Wollaston wires

In addition to the null heat flux condition at the extremity of the fin, the junction with the Wollaston introduces the second limit condition. The corresponding link between the temperature $T(L_p, q\omega)$ and the heat flux $\Phi(L_p, q\omega)$ at the junction Pt–Rh/cone and Wollaston wire is written [15]:

$$T(L_p, q\omega) = \frac{i}{k_p(q\omega)\kappa_p}\frac{1+\mathcal{R}(q\omega)}{1-\mathcal{R}(q\omega)}\Phi(L_p, q\omega) \tag{6}$$

with the *wave vector* k_p given by:

$$k_p(q\omega) = \sqrt{\frac{iq\omega}{\alpha_p} - \frac{2h_p}{r_p\kappa_p}} \tag{7}$$

and where $\mathcal{R}(q\omega)$ is the generalized reflexion coefficient of thermal wave at the junction, due to the presence of the cone and the Wollaston wire [15]. An exchange coefficient along the cone is introduced, varying with the local diameter. Of course, this coefficient is taken to be very small for the vacuum case, corresponding to the linearized radiative exchange, along the lateral surface of the wires.

The multilayer formalism furnishes $\mathcal{R}(q\omega)$ in terms of the corresponding reflection coefficient $\mathcal{R}_W(q\omega)$ at the junction between the cone and the Wollaston wire, taking the wire length and the constriction with the electrical supply into account, along:

$$\mathcal{R}_W(q\omega) = -\frac{h_{\mathrm{ext}} + i\kappa_W k_W(q\omega)}{h_{\mathrm{ext}} - i\kappa_W k_W(q\omega)}\exp(2ik_W L_W) \tag{8}$$

with

$$k_W(q\omega) = \sqrt{\frac{iq\omega}{\alpha_W} - \frac{2h_W}{r_W\kappa_W}} \tag{9}$$

In practice, due to the high value of the h_{ext} coefficient, the important physical parameter in Eq. (8) is the length L_W of the Wollaston wire. Apart from the very low frequencies the electrical supply has negligible influence upon the 3ω response, contrarily to the corresponding DC response. In that concerns the Wollaston wire, it must be noticed that the 3ω response is influenced up to several percents under one hundred hertz and so its influence ought to be considered due to the sensitive experimental response.

3. Experiments and comparisons

3.1. What are the most important parameters?

Even though the thermal parameters are the same everywhere along the bent probe there are numerous parameters having importance for the thermal response description.

Let us precise them:

- exchange thermal coefficients at the air/Pt–Rh wire interface (typical values 1200 and 60 $\mathrm{W\,m^{-2}\,K^{-1}}$ [13] have been chosen respectively for Pt–Rh and the Wollaston wires in air, for the FEM-analytical approaches comparison). One must underline the actual value of these parameters are not exactly known, due to the complicated probe geometry (shape and position with regard to the surrounding air, leading to a difficult analysis of microconvection). On another side, one must ask about the respective validities of the convective and conductive exchanges with the surrounding air, specially in the AC domain;
- physical parameters of the probe: actually, the thermal and electrical conductivities of the Pt–Rh could be different from values given by the constructor, due to structural modifications of the alloy during bending process; the uniformity of their values along the probe is probably a simplifying hypothesis. Moreover, the two conductivities are correlated (for instance the Wiedeman–Franz law for pure metal);
- for the SThM probe it is known that the heat flux generated by Joule effect is for its greatest part evacuated *via* the Wollaston wire [11], and ultimately toward the electrical leads. So the Wollaston part length is one parameter of

modelings: several mm have been measured with an optical microscope. This implies that the Wollaston wire is not surely a perfect heat sink, at least for the small frequencies;
- the two geometrical dimensions (r and L) of the Pt–Rh wire are crucial to describe the response. In particular, the uniformity of the radius r along the wire is a first simplifying hypothesis leading to a rapid analytical calculation.

Thus one discovers that a complete characterization of the thermo-resistive probe is a difficult task.

3.2. FEM vs analytical modeling

The two modeling responses are compared for an identical set of physical data (thermal and geometrical characteristics, imposed AC current), cf. Table 1. The FEM response is characterized by a transient and a permanent AC regimes giving the temperature evolution at each node *vs* the time. Figs. 3 and 4 show calculated temperatures at two different points of the Pt–Rh wire. Analytical results are obtained in the frame of multifrequential approach, using the harmonic responses up to the 4ω component of the temperature field, with a non-negligible part.

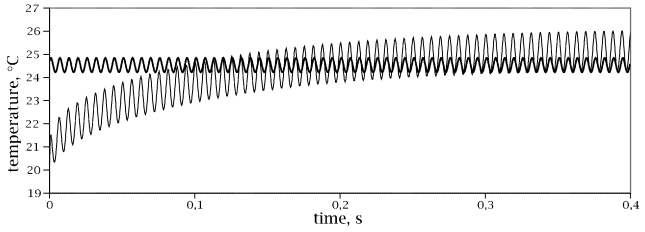

Fig. 3. The average temperature on the cross section of the Pt–Rh probe, at the junction with the Wollaston, for a 50 mA cosine current, at 80 Hz, heating the probe from $t = 0$ s. Thin curve: FEM approach; bold curve: analytical method; the temperature of the fin model at the Pt–Rh/cone junction.

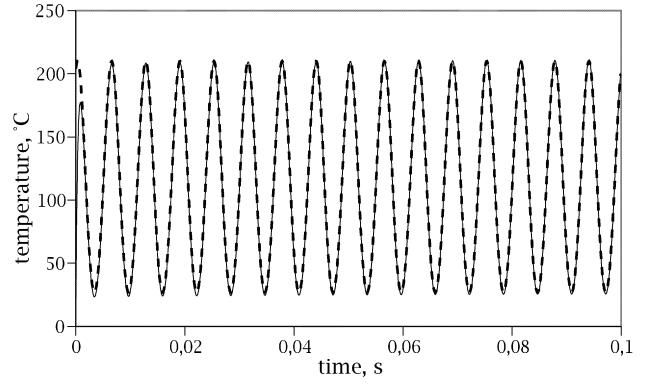

Fig. 4. The average temperature on the cross section at the extremity of the probe, for a 50 mA cosine current, at 80 Hz. Plain curve: FEM response; dashed curve analytical result.

The figures complete the first coherent results given in Refs. [10,16].

Fig. 3 shows the temperature at the Pt–Rh/Wollaston junction. The FEM results show clearly the transient and permanent behaviors of the average temperature value in the cross section, taking the perturbing heat sink (Wollaston wire) into account; the analytical method introduces only the permanent regime. These approaches differ a little in the AC temperature amplitude; the phases are similar. Thus, for this small frequency, the junction is not a pure heat sink (small oscillating temperature, around 5 °C higher than the ambient temperature (20 °C)). For higher frequencies (some hundreds Hz) the Pt–Rh/Wollaston wire junction can be interpreted as an AC perfect heat sink: this is due to the short heat diffusion length (Eqs. (6) and (8)).

At the other extremity of the Pt–Rh part, the average temperature on the cross section is shown on Fig. 4; the permanent regime is reached in some thousandths of a second.

It has been verified that apart from the very vicinity of the Pt–Rh/Wollaston junction the two approaches give comparable results, in amplitude and phase, giving confidence to validity of the fin modeling analysis. A Fourier analysis of the FEM response can be easily obtained and compared with the analytical method. This agreement shows that Eqs. (4) and (5) are directly suited for a comparison with the bridge voltage.

Fig. 5 presents analytical responses $f(\omega) = V_{3\omega}/I_b^3$ [7,16] for three currents (10, 33 and 50 mA), leading to important variations of the average temperature. For the air conditions, the exchange coefficient has been adapted for each current (average temperature) [13]: 700, 800 and 1150 $\mathrm{W\,m^{-2}\,K^{-1}}$ for the 10.04, 33.11 and 50.86 mA current, respectively; for the vacuum case, the values 7, 11 and 13 $\mathrm{W\,m^{-2}\,K^{-1}}$ have been retained. For a given current the role of exchange coefficient is enlightened by the lowering of the amplitude curve, specifically at low frequencies. In the vacuum case, the exchange coefficient have little influence, and the differences between the corresponding curves illuminates a result of the multifrequential approach: $V(3\omega)/I_b^3$ is a function of I_b, contrary to the result given in Ref. [16].

3.3. Experimental results

The electrical circuit presented on Fig. 1 is excited with the internal generator $V_S(1\omega)$ of a lock-in amplifier (up to 2 V (rms)), amplified ($\times 4$) by an home-made device (with a well defined phase and amplitude response). The resistor R_1 has been chosen with a relatively large value (217.9 Ω) compared to the probe resistance ($R_p + R_{\mathrm{ext}} \approx 2\ \Omega$) such that only small variations are induced by the thermo-resistive behavior of the Pt–Rh part. This permits the assumption that the probe is supplied with a constant AC current (that is a condition of the 3ω method) [7]. The second leg of the bridge (resistors R_3 and R_4)

Table 1
Values of the geometrical and thermo-physical parameters of the Pt–Rh probe that serves as references

L [m]	r [m]	κ [$\mathrm{W\,m^{-1}\,K^{-1}}$]	α [$\mathrm{m^2\,s^{-1}}$]	ρ_a [Ω m]	ε [$\mathrm{K^{-1}}$]
100×10^{-6}	2.5×10^{-6}	37.6	1.32×10^{-5}	19×10^{-8}	1.66×10^{-3}

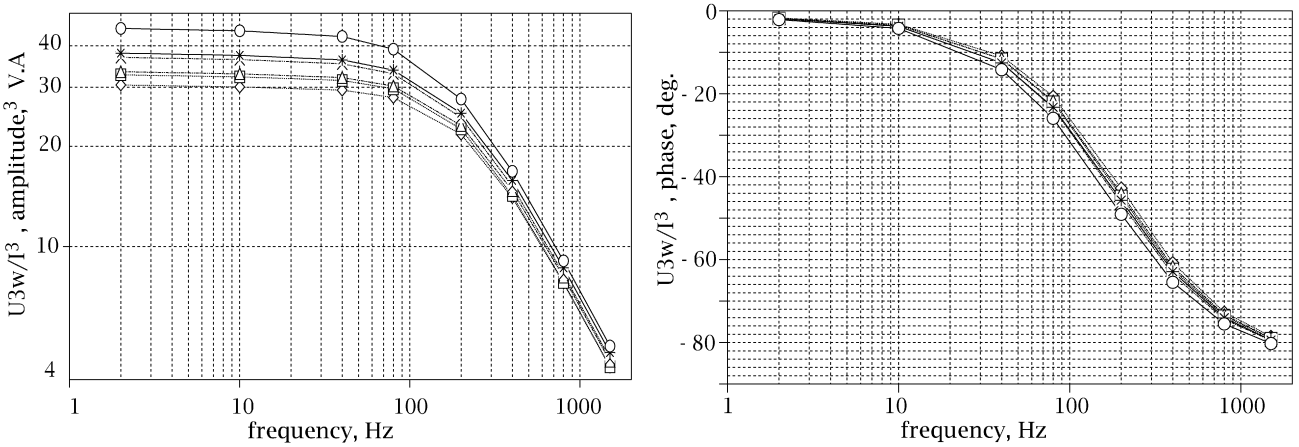

Fig. 5. Theoretical approach for the ratio $V_{3\omega}/I_b^3$. The six curves correspond to three different currents, with two conditions, air or vacuum, respectively: (10.04 mA, rhombus and squares; 33.11 mA, triangles and crosses; 50.86 mA, stars and circles). Left—amplitude of the $V_{3\omega}/I_b^3$ signal. Right—phase of the $V_{3\omega}/I_b^3$ signal.

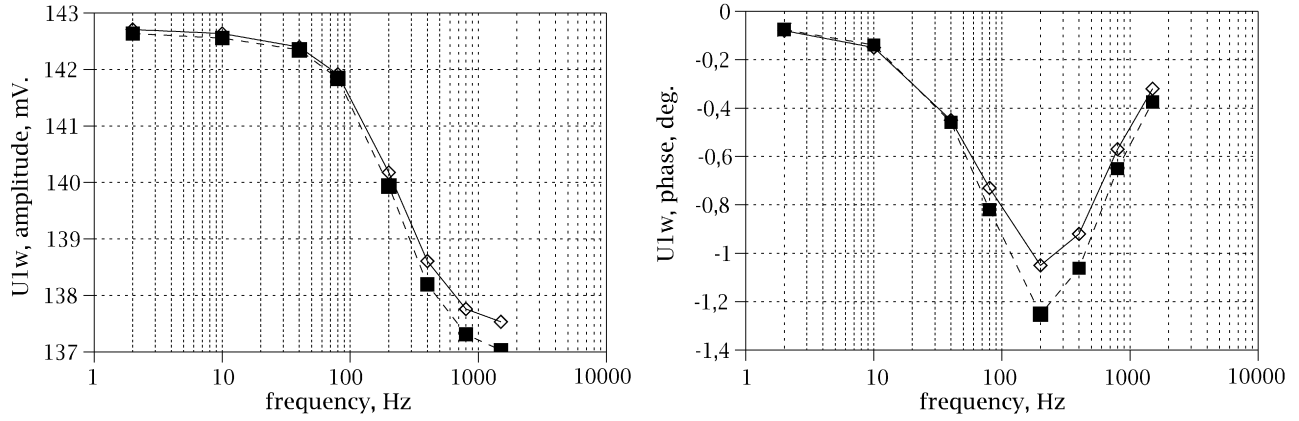

Fig. 6. Left—amplitude of the 1ω signal: the direct measurement of the signal (empty rhombus) is compared with a theoretical approach (plain squares). Right—phase of the 1ω signal.

is chosen such that the Wheatstone bridge is balanced for the $V_{1\omega}$ component (cf. Fig. 1). The voltage can be measured directly between the probe terminals, or between the points A and B. The second possibility is preferred for the harmonic responses at 2ω, 3ω, ..., giving a high S/N ratio; the first one will give the fundamental response.

It must be underlined that experiments with the probe in air or vacuum without contact with sample reveal very stable and repetitive signals. However for the higher harmonics that have been studied here (5ω), a perturbative influence of the electrical circuit has been encountered.

Although the analytical modeling is worthwhile for any AC or DC cases, all the studies presented here use only a pure sinusoidal source.

3.4. Comparison modeling—experiment

The first comparison showing the interest of the multifrequential approach is obtained with the study of 1ω signal, between the probe terminals, for $I_b = 50.86$ mA, in air (Fig. 6). For such a current, the variations of the average temperature *vs* frequency are sufficiently high that $V_{1\omega}$ variations are induced. At this stage a crude fit has been only used, firstly in choosing the probe parameters from a minimization on the 3ω response (see *infra*), and secondly in choosing the value of electrical resistance in series with the Pt–Rh part (cf. Fig. 1), giving the entire resistance that is actually measured. Note that this resistance shows a little variation from one current to another [3]: typically we obtain 0.5–0.6 Ω.

It appears that this response (amplitude and phase) at the fundamental frequency can be easily explained with the aid of Eqs. (4) and (5).

It must be underlined that the electrical current must be precisely controlled. This can be obtained in using precise amperemeter, or an indirect evaluation from the source voltage and the knowledge of the different resistances. Actually, as it can be suggested on Fig. 6, the probe voltage varies on the entire spectrum. However one can verify that this corresponds to variations of the probe electrical resistance with the average temperature at each frequency. Our probe has shown resistances (the probe only) from 2.14 to 2.40 Ω for currents from 0 to 51 mA. This implies a small relative variation of the current (approximatively one thousandth, for the upper values): whatever the frequency and the current are, the measurements are made in the conditions of the 3ω method.

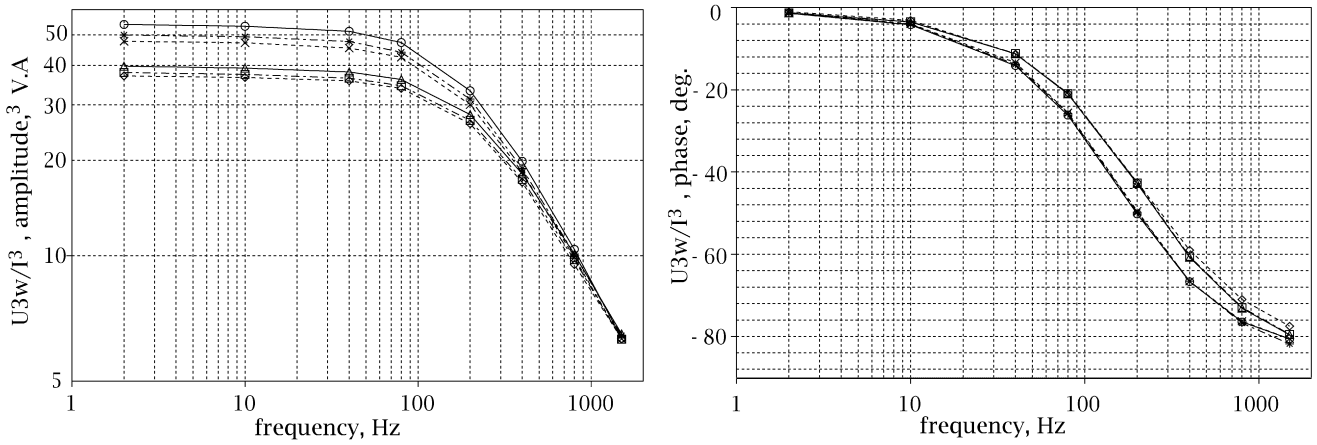

Fig. 7. Experimental results: The six curves correspond to three different currents, with two conditions, air and vacuum, respectively: 10.04 mA, rhombus and crosses; 33.11 mA, squares and stars; 50.86 mA, triangles and circles. Left—amplitude of the $V_{3\omega}/I_b^3$ signal: the curves are clearly separated at low frequencies. Right—phase of the $V_{3\omega}/I_b^3$ signal.

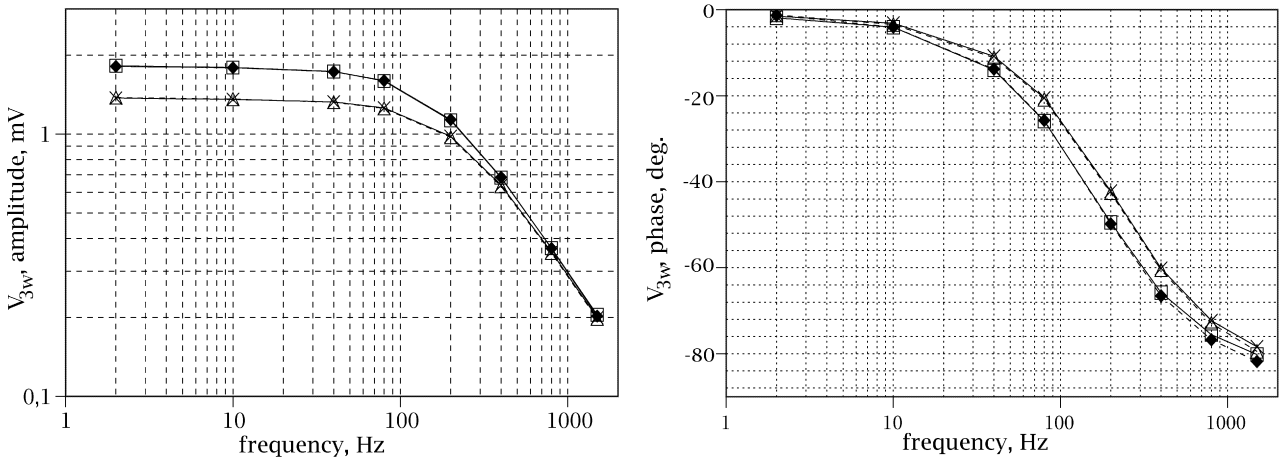

Fig. 8. Minimization on $V_{3\omega}$ from the 33.11 mA data, vacuum. The parameters length and radius are estimated for a given thermal conductivity and an exchange coefficient in vacuum (empty squares and plain rhombus, experimental data and minimized results). The results are applied for the same current in air for the exchange coefficient determination (empty triangles and crosses). Left—amplitude of the $V_{3\omega}$ signal. Right—phase of the $V_{3\omega}$ signal.

Fig. 7 shows the $V(3\omega)/I_b^3$ signal taken between points A and B: it appeared that, for the smaller current (10.04 mA, leading to a small increase of the probe average temperature (some °C)), the measured voltage is only of several tens μV, and that the direct measurement can be unstable, particularly the phase. For high frequencies the temperature amplitudes coincide, although the phases show (for frequencies up to 1500 Hz) some differences between behaviors in vacuum or in air. In vacuum case, the heat is in practice totally evacuated by wires; this gives importance to the diffusion length of thermal wave. In air case, the heat is partially given to the ambient air: this leads to a local exchange, diminishing the phase delay. However, a simple comparison of Figs. 5 and 7 reveals the necessity of a clarification of the modeling hypothesis.

3.5. Minimizations and discussion

The following step consists in using the model in a least-square procedure, to estimate from measurement the geometrical and thermal parameters. As a first approach the minimizing procedure "fminsearch" implemented in Matlab® has been used. That multisimplex 0-order algorithm converges slowly, but it allows crude initial conditions, and is not affected by the strong correlations between the parameters.

The routines have been performed on numerous set of experimental results, corresponding to different conditions, vacuum or air, for three currents: 10.04, 33.11 and 50.86 mA. It must be underlined that the ambient temperature must be controlled and is integrated in the analytical model.

For the present, we have considered several steps that are presented below, using the 3ω results.

Firstly, thermo-physical parameters of the probe are supposed constant (cf. Table 1). The minimization is done with respect to the geometrical parameters (length and radius) in the case 33.11 mA, vacuum. In that concerns the exchange coefficient in vacuum, a simple linearization from the Stefan's law has been done, evaluated for the obtained average probe temperature, along an iterative calculation using the model itself (7 to 13 $\mathrm{W\,m^{-2}\,K^{-1}}$). In practice, for the vacuum case, this small value has no importance, because it is known [10,17] that

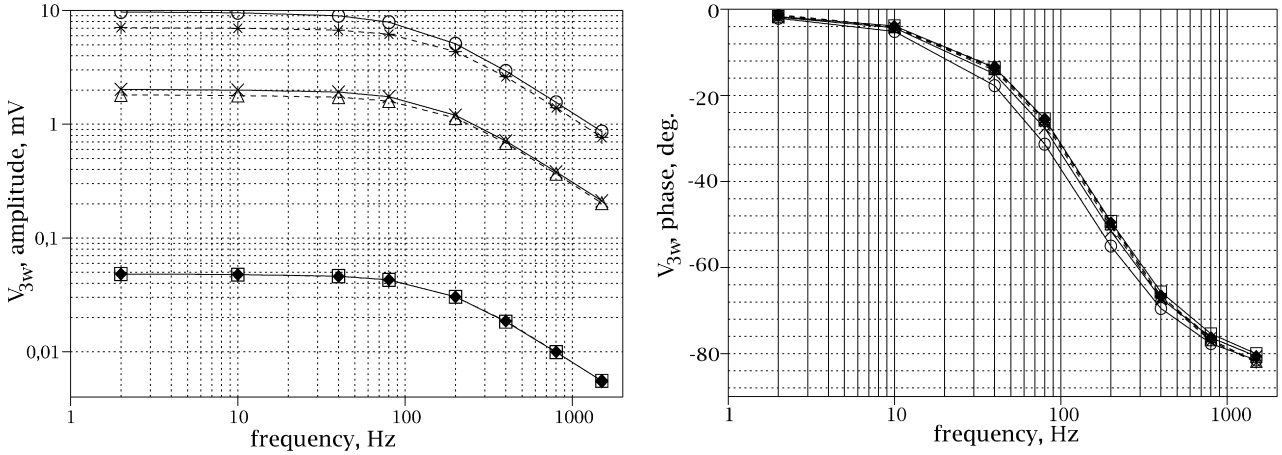

Fig. 9. Minimization from the 10.04 mA data, vacuum case. The parameters length, radius and thermal conductivity are estimated for the 10.04 mA, in vacuum (experimental data and minimized results: squares and rhombus). The results are applied for other currents, in vacuum case (33.11—triangles and crosses—and 50.86 mA—stars and circles). Left—amplitude of the $V_{3\omega}$ signal. Right—phase of the $V_{3\omega}$ signal.

in case of the SThM probe the heat flux is evacuated principally *via* the Wollaston wire.

On Fig. 8 the minimized and experimental results concerning the case 33.11 mA, at first in vacuum, next in air, are compared. The minimization (33.11 mA, vacuum) leads to $L = 119.4$ μm, $r = 2.65$ μm, which are then applied in case of the (33.11 mA, air) for a second minimization on the exchange coefficient. Each of the two cases corresponds to two curves, practically superposed, that could indicate a great agreement. The amplitude curve reveals the vanishing influence of exchange coefficient in increasing frequency; the phase one shows the role of exchange coefficient, giving local heat flux out of the probe, diminishing the phase delay. The problem is here that the agreement for the air case is obtained with an exchange coefficient as high as 2300 $\mathrm{W\,m^{-2}\,K^{-1}}$, which is 3 times the value given by usual correlations [9,10]. Moreover, this geometry (r and L) appears invalid for other currents.

The second study Fig. 9 begins by a minimization in the vacuum case (10.04 mA), with the possibility of varying length, radius and thermal conductivity. The obtained values are $L = 114.58$ μm, $r = 2.625$ μm and $\kappa = 32.38$ $\mathrm{W\,m^{-1}\,K^{-1}}$. These results give an approximative agreement for the case (33.11 mA, vacuum) and a poor one for the case (50.86 mA, vacuum); in particular, experimental amplitudes appear lower than the corresponding analytical results.

It must be underlined that such a minimization independently made for each current gives sets of values showing similar, but not identical, characteristics. Of course, this can be the signature of the correlation between the different parameters: in a following step of this work, it will be essential to calculate the estimated parameters variance, depending of these correlations. Let us note here that the hypothesis of an increasing thermal conductivity of the Pt–Rh alloy with the temperature will permit to bring closer together the minimized and experimental curves on Fig. 9, as it could explain the differences between the theoretical and experimental $V_{3\omega}/I_b^3$ curves (Figs. 5 and 7). Moreover, due to the temperature profile along the probe, this temperature effect on the thermal conductivity implies naturally to the necessity a local description of the parameters. This could be incorporated partly in a refined version of the present analytical modeling. Of course, the temperature profile introduces also a local exchange coefficient: this leads to a complicated microconvection around the probe in air, due the important amplitude of the AC temperature field obtained for the higher current. These points are important for an accurate description of the contact with a sample, the interesting zone being currently the warmer part of the probe.

4. Conclusion

The complicated behavior of the local thermal probe used in the SThM AC experiments necessitates the consideration of many geometrical and thermal parameters that induce the temperature and the voltage responses. Before a minute analysis of the thermal flux conditions through the contact with a sample, the characterization of the probe is a first step. This supposes that one has at one's disposal an efficient method for the treatment of the experimental data. In the present case an analytical modeling has been developed such as to work out the appropriate parameters.

The complete AC multifrequential modeling has been validated by comparisons with the FEM approach and, qualitatively, with different harmonics of the out-put signal. Then, we used it in a leastsquare minimization procedure, in order to estimate the geometrical and thermal parameters. It appears that the estimated values depend on the electric current intensity (or on the average temperature). This result occurs whereas the different minimizations have been begun with different initial values for the parameters: they have shown a good convergent stability. This leads to the conclusion that despite its improvements, some parts of the modeling are not sharp enough. For instance, thermal conductivity and exchange coefficient profiles along the probe ought to be introduced.

However, the present work enlightened several points that must be considered for the DC or low frequency AC experiments. The junction with the soldering, in practice here the Wollaston wire, must be taken into account. This underlines

the long distance influence of the temperature field in the local thermal probes use. On a general ground, the multifrequential approach can be extended beyond the case of the thermal fin to different geometries, as the electrical stripes deposited on materials for the use of the 3ω method.

On another side, the different thermal and geometrical parameters are correlated, as its appears on the heat Fourier equation. Independent measurements of some of these parameters would be beneficial; perhaps ideally, repetitive making of thermal probes will eliminate the necessity of the probe characterization.

References

[1] S. Lefèvre, S. Volz, 3ω-scanning thermal microscope, Rev. Sci. Instruments 76 (2005) 033701.
[2] G.B.M. Fiege, A. Altes, R. Heiderhoff, L.J. Balk, Quantitative thermal conductivity measurements with nanometre resolution, J. Phys. D: Appl. Phys. 32 (1999) L13–L17.
[3] L. Lu, L. Yi, D.L. Zhang, 3ω method for specific heat and thermal conductivity measurements, Rev. Sci. Instruments 72 (2001) 2996–3003.
[4] B.W. Olson, S. Graham, K. Chen, A practical extension of the 3ω method to multilayer structures, Rev. Sci. Instruments 76 (2005) 053901.
[5] D.G. Cahill, Thermal conductivity measurement from 30 to 750 K: the 3ω method, Rev. Sci. Instruments 61 (1990) 802–808.
[6] T. Borca-Tasciuc, R. Kumar, G. Chen, Data reduction in 3ω method for thin-film thermal conductivity determination, Rev. Sci. Instruments 72 (2001) 2139–2147.
[7] Ch. Dames, G. Chen, 1ω, 2ω and 3ω methods for measurements of thermal properties, Rev. Sci. Instruments 76 (2005) 124902.
[8] S. Lefèvre, S. Volz, P.-O. Chapuis, Nanoscale heat transfer at contact between a hot tip and a substrate, Int. J. Heat Mass Transfer 49 (2006) 251–258.
[9] S. Gomès, Contribution théorique et expérimentale à la microscopie thermique à sonde locale : calibration d'une pointe thermo-résistive, analyse des divers couplages thermiques, Thèse, Université de Reims, 1999.
[10] S. Lefèvre, S. Volz, J.-B. Saulnier, C. Fuentes, N. Trannoy, Thermal conductivity calibration for hot wire based dc scanning thermal microscopy, Rev. Sci. Instruments 74 (2004) 2418–2423.
[11] J.-F. Henry, N. Trannoy, Microscopie thermique à sonde locale (SThM) : analyse expérimentale des échanges thermiques sonde-écahntillon par thermographie infrarouge, in : Congrès Société Française de Thermique, 2003.
[12] H.S. Carslaw, J.C. Jaeger, Conduction of Heat in Solids, Oxford University Press, London, 1965.
[13] V.T. Morgan, The overall convective heat transfer from smooth circular cylinders, in: Advances in Heat Transfer, vol. 11, Academic Press, New York, 1975, pp. 199–212.
[14] F. Depasse, Ph. Grossel, N. Trannoy, Probe temperature and output voltage calculation for the SThM in AC mode, Superlat. Microstruct. 35 (2004) 269–282.
[15] Ph. Grossel, F. Depasse, N. Trannoy, Multicouches thermiques et profils thermophysiques continus : une approche récursive, J. Phys. III France 7 (1997) 13–33.
[16] S. Lefèvre, J.-B. Saulnier, C. Fuentes, S. Volz, Probe calibration of the scanning thermal microscope in the AC mode, Superlat. Microstruct. 35 (2004) 283–288.
[17] S. Gomès, F. Depasse, N. Trannoy, Ph. Grossel, C. Bainier, D. Charraut, DC scanning thermal microscopy: characterization and interpretation of the measurement, Int. J. Thermal Sci. 40 (2001) 949–958.